Optimal shaft-hub connections

Leergaard Pedersen, Niels

Published in:
Journal of Strain Analysis for Engineering Design

Link to article, DOI:
10.1177/03093247221080016

Publication date:
2023

Document Version
Peer reviewed version

Optimal shaft-hub connections

Niels Leergaard Pedersen
Dept. of Mechanical Engineering, Solid Mechanics
Technical University of Denmark
Nils Koppels Allé, Building 404, DK-2800 Kgs. Lyngby, Denmark
email: nlp@mek.dtu.dk

Abstract

In all power transmitting machines the shaft-hub connection has a large impact on the overall machine size, if the strength can be increased we can reduce the size. The connection between shaft and hub is a machine element with many possible designs available and described in standards. The connection can be either permanent or changeable, the goal is in all cases to have as high a strength for the connection as possible. Focus is in the present paper on the connections with easy assembly and disassembly, i.e. on positive connections (geometrically locked). The designs specified in standards are traditionally made with straight lines and circular arches. Alternatively the involute spline can be used. For this case the cutting tool shape is made with straight lines and circular arches. Present standard designs are not made with minimum stress concentrations as the main objective, other features as e.g. easy manufacturing has the primary importance. In the present paper we show how the involute spline design can be significantly improved in relation to strength maximization by reducing the maximum stress. The maximum stress can in many cases be reduced by more than 54% relative to standard design.

Machine elements, involute, spline connection, torsion, stress concentration, FEA, 2D/3D.

1 Introduction

In order to reduce the overall power transmitting machine dimensions the individual component strength must be increased, one possibility for this is to use optimization methods. The involved machine elements strength is typically controlled by the fatigue strength.

One of the primary machine element components used in power transmitting machines is the shaft hub connection. The torque can either be transferred between the two components by friction or by normal load, the latter is typically selected if demountability is important. The present paper focus is on positive connections, i.e. where there is a normal load between the shaft and hub due to a geometric locking of the two parts. The paper does not include coupling connections. The most simple form of these connections is a pin or a key joint see e.g. (DIN 6885-1 1968) for a standard design definition of the key and keyway. The strength of key connection is limited although design improvement by using optimization methods is possible see e.g. (Pedersen 2010). If one key does not have sufficient strength more keys can be added, but typically it is preferred then to use a spline. The design of splines also have a number of different standard designs. The simplest design is the straight sided design see e.g. (DIN ISO 14 1986). In (Pedersen 2011) it is shown that also for the case of straight sided splines it is

possible to make smaller shape modifications that has a significant influence on the strength. Today the preferred design of splines is probably the involute spline, i.e. where the design is the same as for the involute gear, typically with a pressure angle of 30° (instead of 20° which is the preferred pressure angle for gears), see (DIN 5480-1 2006) and (DIN 5480-16 2006). In relation to gears the involute shape has some clear advantages making this the preferred shape, e.g. that the moment arm is constant for all contact points on the teeth. The reason for using the same shape in spline design is the distribution of the load across the involute but also the high production precision of the shape.

The torque is transferred in the connection due to contact stress. In the present paper we will assume that the connection is loaded by a pure torsionally load. Assuming the stress (load) to be constant, the highest torque is achieved when the load direction is perpendicular to the position vector, i.e. the vector from the shaft centre to the load point. For a straight sided spline (straight sided tooth profile) the load is almost perpendicular to the position vector. The angle between position vector and direction of stress or load is also typically termed the pressure angle as seen in e.g. (Pedersen 2021) and references there-in related to polygon/trilobe design. In gear design the pressure angle is defined for the pitch point as the angle between a vector perpendicular to the position vector and the direction of normal force. It is seen that the two definitions of the pressure angle is different but at the pitch point the sum of the two angles is $\pi/2$. The problem in using straight sided splines is, e.g. the high stress concentrations associated with this design.

The fatigue strength evaluation of a shaft hub connection is performed by finding the maximum stress in the connection, most typically controlled by a stress concentration. In relation to splines the stress evaluation can be found in e.g. (Yoshitake 1962) and (Benatar, Talbot & Kahraman 2017) using experimental methods and in (Leykin & Starichneva 1975) and (Wink & Nakandakari 2013) using analytical methods. Evaluation using finite element methods (FEM) can be found in e.g. (Volfson 1982), (Kahn-Jetter & Wright 2000), (Chase, Sorensen & Decaires 2010), (Barsoum, Khan & Barsoum 2014) and (Wendler & Schlecht 2016). Using FEM the axial stress distribution is also discussed in (Tjernberg 2001) and (Barrot, Paredes & Sartor 2009). In (Kahn-Jetter, Hundertmark & Wright 2000) the involute spline strength is compared to the strength of a trilobe design. In the present paper we apply the finite element method (FEM) for stress evaluation. The loading condition is assumed to be pure torsional.

In relation to splines we also have a problem related to tolerances in that it will typically not be all teeth that come into contact initially, see e.g. (Hong, Talbot & Kahraman 2015). The evaluation of this point is not straight forward using FE, and this is primarily a problem if the material is brittle.

Design improvements or optimization directly related to the involute spline connection is to the authors knowledge not found in any papers. Optimization of the involute shape can be found but then primarily relates to gear design see e.g. (Pedersen 2015) and references there-in. Generally there is a great potential for using design optimization for machine elements. To ensure that different elements can be connected and to have an overall high element strength most designs are defined in different standards. This makes the industry conservative in that there is a reluctance to use new designs. Some of this reluctance is given by the production but today larger variations are possible with the geometric design taken directly from computer models (CAD/CAM). Examples of optimization of other standard machine elements can be found in e.g. (Pedersen 2016) and (Pedersen 2019). Focus in the present paper is on the practical aspects of the proposed designs. Practical being seen as either the proposed new designs should work with existing standard designs or/and that the design shape has an easy mathematical parameterization.

The paper is organized as follows. In Section 2 the problem is defined. The standard involute

design is examined for comparison in Section 3. Section 4 discusses the difficulties in using FE to model torsion between shaft and hub including contact analysis. The optimized results are presented in Section 5. Finally the conclusions are given in Section 6.

2 Definitions

For the positive connection definition we first need to define or select the symmetry angle or equivalent the number of teeth in the connection. In Figure 1 different standard designs are shown for illustration. Figure 1a is an example where the symmetry angle is 2π. The designs in Figures 1b and 1c are maybe not so common; here the symmetry angles are $2\pi/3$ and $2\pi/4$ respectively, see (Pedersen 2021) for more details also in relation to optimization. In Figure 1d the design of an involute spline according to (DIN 5480-1 2006) is shown; here the number of teeth is 32 and therefore the symmetry angle is $\pi/16$.

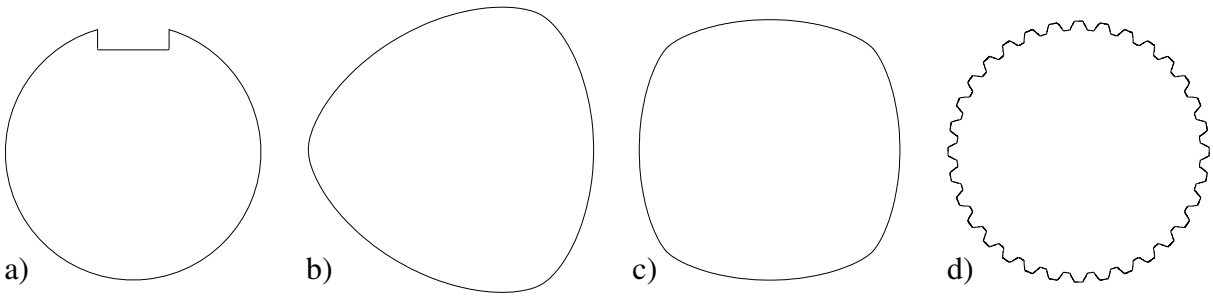

Figure 1: Cross section of shaft design for different positive connections. a) Parallel keyway, according to (DIN 6885-1 1968) b) Polygon profile as specified in (DIN 32711 1979) (P3G). c) Polygon profile as specified in (DIN 32712 1979) (P4C). d) Involute spline as defined in (DIN 5480-1 2006).

The strength of a shaft hub connection is related to fatigue failure and therefore the reduction of maximum stress is the focus of an optimization. The maximum stress is found typically at singularity point in relation to contact or at abrupt changes in geometry or shape where we have stress concentrations. The practical designs in Figure 1 are all cross sectional designs (2D). There will also be 3D effects due to the run-out of these designs, e.g. for the parallel key we have the possibility for a profile keyway or a sled-runner keyway. In the present paper the focus is on the stress resulting from the prismatic part because this is the most generic, many different options are possible for the transition or run-out to a circular shape.

For positive connections where we have a geometric lock between shaft and hub the torque is primarily transferred by the normal contact stress between the two parts, contrary to an interference fit where the torque is transferred by friction.

The primary shape of the involute spline is the involute shape that is also found in standard gear design. The shape can mathematically be given as

$$\left\{ \begin{array}{c} x(s/r_b) \\ y(s/r_b) \end{array} \right\} = \left[\begin{array}{cc} \cos(s/r_b) & -\sin(s/r_b) \\ \sin(s/r_b) & \cos(s/r_b) \end{array} \right] \left\{ \begin{array}{c} r_b \\ -s \end{array} \right\} \tag{1}$$

where the free parameter is the arc length, s, the base circle radius r_b is given by

$$r_b = M\frac{z}{2}\cos(\alpha) \tag{2}$$

here M is the module (a constant that defines the tooth height), z is the number of teeth and α is the pressure angle that for standard involute splines is fixed at $\alpha = \pi/6$. The base circle and the involute geometry is shown in Figure 2, here the normal force F_n and the frictional force F_f are also shown.

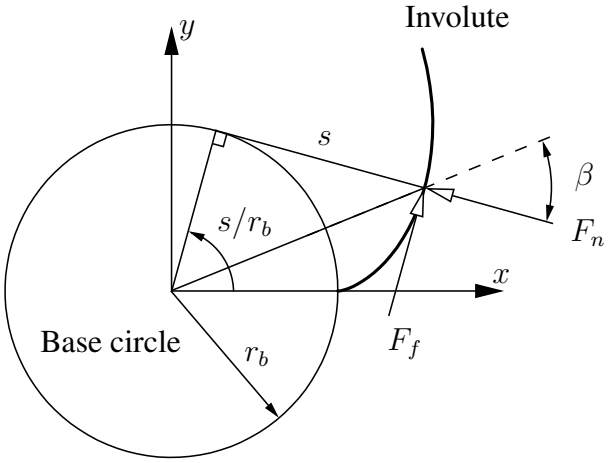

Figure 2: Base circle and involute geometry, the angle is defined by the base circle arc length s.

In Figure 2 we also show the angle β that in relation to trilobe design has been termed the pressure angle, see e.g. (Czyzewski & Odman 1988), this angle is not constant and will depend on the position on the involute. In the present paper we will, as done for gear design, term the angle α the pressure angle.

The torque transferred by the two forces is

$$T = F_n r_b + F_f s \tag{3}$$

where the maximum possible friction force value is $F_f = \mu F_n$, assuming Coulomb friction. The angle β is given by

$$\sin(\beta) = \frac{r_b}{\sqrt{r_b^2 + s^2}} \tag{4}$$

The pitch point on the involute is where the curve intersects with the circle with the reference radius

$$r = M\frac{z}{2} \tag{5}$$

This leads to that

$$s = \sqrt{r^2 - r_b^2} \tag{6}$$

and therefore for the pitch point we have that

$$\sin(\beta) = \cos(\alpha) \qquad \Rightarrow \qquad \alpha + \beta = \frac{\pi}{2} \tag{7}$$

The objective for improving the strength of a shaft hub connection is to reduce the maximum stress for a given torque level. From Figure 2 we see that the larger the angle beta is the higher is the torque that can be transferred for a given normal load at a given position. For a straight sided spline we have that β is approx. $\pi/2$ and the torque is transferred primarily by F_n, for an interference fit we have that $\beta = 0$ and the torque is transferred only by F_f.

The maximum value of F_f is given by the friction coefficient and a conservative guess for steel-steel contact is $\mu = 0.1$. For an interference fit we do not have a stress concentration but because the torque is transferred by F_f we need a high value of F_n although this does not contribute directly to the transferred torque. At the other end of possibilities we have the straight sided spline where the force F_n can be considerable smaller for transferring the same torque, for this case we will however due to the design have a high value for the stress concentration. For the practical design of shaft-hub connection it is therefore a balance between the two outer limiting cases that can give the optimal design.

3 Standard involute design

The shape of the involute part of the involute spline is as given in (1), i.e. in analytically form. The transition from the involute to the tooth root is however not given analytical. This shape is the result of the cutting tool used for the production, as it is also the case for gears. This part of the design is very important since stress concentrations are likely to be in this part. In the involute spline design we have an external gearing on the shaft and an internal gearing in the hub. The shaft teeth can be cut by a rack cutter but this is not possible for the internal gearing in the hub, here a gear cutter must be used. In the standard (DIN 5480-16 2006) the standard pinion gear cutter design is specified by the design of a standard cutting rack. In order to establish the involute spline design we therefore first have to find the pinion gear cutter design. This gear cutter can then be used to cut both the external gear and the internal gear. The design resulting from a cutting tool (rack cutter or gear cutter) can be estimated in many ways, in the present paper we will apply the numerical method presented in (Pedersen 2015) to find the wrapping curve. In (Pedersen 2015) also an analytical method for finding the wrapping curve can be found.

If we select a Module $M = 3\mathrm{mm}$ and a reference connection diameter to be $d_B = 100\mathrm{mm}$. We have according to (DIN 5480-16 2006) a pinion gear cutter with 16 teeth and the shaft and hub should have 32 teeth. The rack cutter teeth shape is as given in Figure 3, and the resulting pinion gear (used as cutter) is shown in Figure 4.

With the pinion gear cutter defined we can find the shaft and hub design. In Figure 5 the combined design of shaft and hub is shown for the case with no profile shift. The shaft is shown in light grey and the hub in dark grey, the full shaft design is seen in Figure 1d. In Figure 5 the points with potentially high stress are indicated as points a, b, c and d. In points b and c there is a singularity in the contact that will lead to high contact stress and in points a and d the shape change results in a stress concentration. It is clear that shape optimization can be applied to the points a and d to reduce the stress concentration. For the points b and c the method of reducing the stiffness at the contact run-out as presented in (Pedersen 2016) can be used.

In keeping the involute design we only need this to be the case between points b and c in Figure 5, for the remaining part we have in principle total design freedom, i.e. where there is no contact between the shaft and hub. For the design in Figure 5 we see that this is a case of flange centered design. Modifications to the design could be made to have internal or external centering by removing either of the shown gabs, this would however require an increased clearance in the contact.

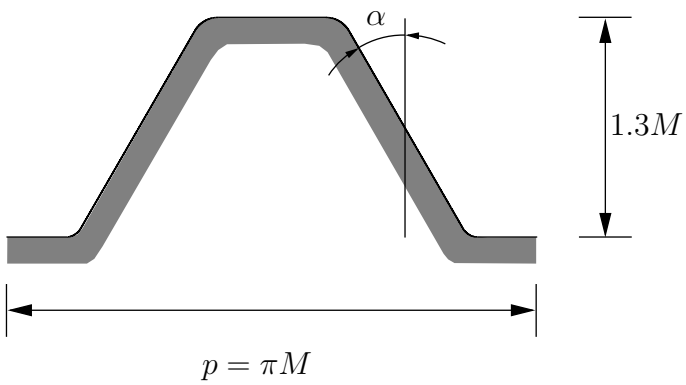

Figure 3: Rack cutter for pinion gear cutter, from (DIN 5480-16 2006). The pitch p is indicated together with the pressure angle α and the tooth height.

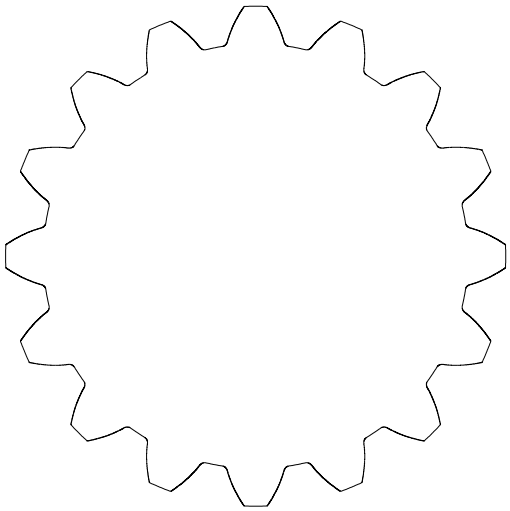

Figure 4: Pinion gear (used as cutter), $z = 16$, $M = 3\mathrm{mm}$, from (DIN 5480-16 2006)

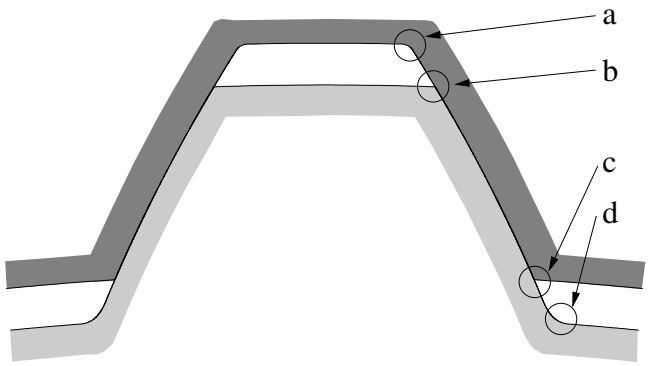

Figure 5: Spline connection teeth of shaft and hub, $z = 32$, $M = 3\mathrm{mm}$, from (DIN 5480-16 2006). For the full shaft see Figure 1d. In the figure the 4 points with potential high stress is shown.

We have now established the design of both hub and shaft for the involute spline. Next the stress resulting from the torsion is evaluated. If the contact is neglected and we assume pure torsion (the shaft and hub can then be analysed separately) the method of using the warping function as defined by Saint-Venant can be applied, see e.g. (Pedersen 2011). In the present

paper however the full modelling of torsion including the contact modelling is preferred and presented in the next Section.

4 Modelling torsion by finite elements

In the present paper the analysis is done numerically using the finite element method. The numerical tool COMSOL (COMSOL AB 1986 -) is used and the contact is modelled using the penalty method and the convergence of the contact modelling is performed by COMSOL. Throughout the paper the material data used is

$$E = 2.1 \cdot 10^{11}\mathrm{N/m}^2, \qquad \nu = 0.3$$

where E is modulus of elasticity and ν is Poisson's ratio.

For the first example we use the spline as defined in the previous section. The selected diameter makes a comparison to the trilobe design in (Pedersen 2021) possible. The torque is therefore selected to be

$$T = 200\mathrm{Nm}$$

The stress is shown as a stress concentration factor defined as

$$K_{vM} = \frac{\sigma_{max}^{vM}}{\sigma_{nom}^{vM}} \tag{8}$$

where σ_{max}^{vM} is the maximum von Mises stress and the nominal von Mises stress is defined relative to a circular shaft, i.e.

$$\sigma_{nom}^{vM} = \sqrt{3}\frac{16T}{\pi d_B^3} \tag{9}$$

In the shaft hub connection we have a three dimensional stress case. For illustration the involute spline defined in the previous section is used here. The hub width is set equal to the reference diameter, i.e. $100\mathrm{mm}$. Due to symmetry we only model one tooth and only one half of this (in axial direction), so in this case only $1/64$ of the full design is used. The hub is clamped at the outer surface and a linear varying distributed shear force is applied to the shaft end. At the shaft and hub centre plane in the axial direction a symmetry condition is applied, and finally a cyclic symmetry conditions are put on the shaft and hub sides. The positions of the boundary condition and the shear load are illustrated in Figure 6. In Figure 7 the result of a 3D contact modelling is shown for the involute spline. In Figure 7 the von Mises stress is scaled by the nominal von Mises stress (9). In the modelling the spline tooth extends across the whole shaft length to avoid the influence from run-out.

In Figure 7 we see that for this case we have a stress concentration factor $K_{vM} = 3.34$, the high stress occurs in the hub at outer surface where we have a singularity in the contact between shaft and hub, corresponding to point c in Figure 5. We notice that the highest stress is very localized indicating that this is not optimal. The stress concentration size is depending on a large number of factors, and especially this is also the case at points of singularity.

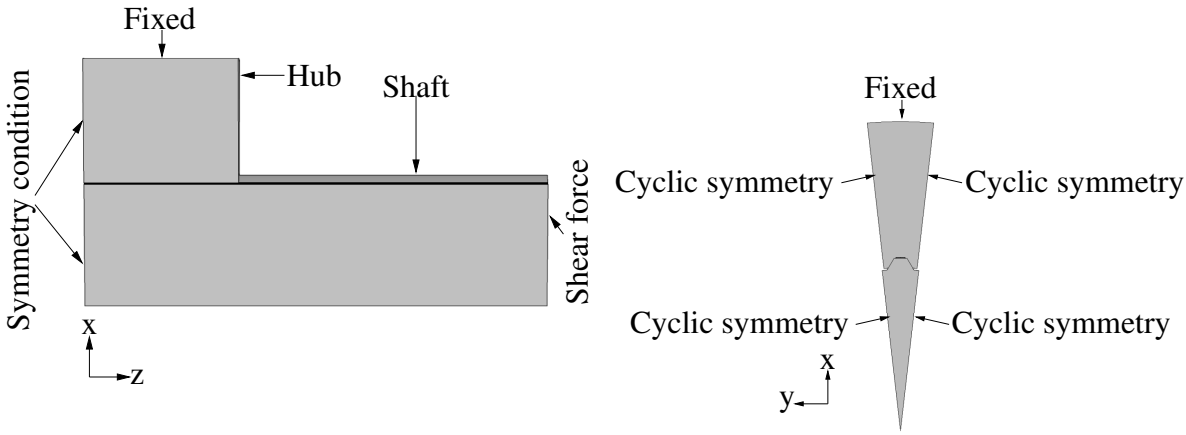

Figure 6: Illustration of placement of FE boundary conditions and load.

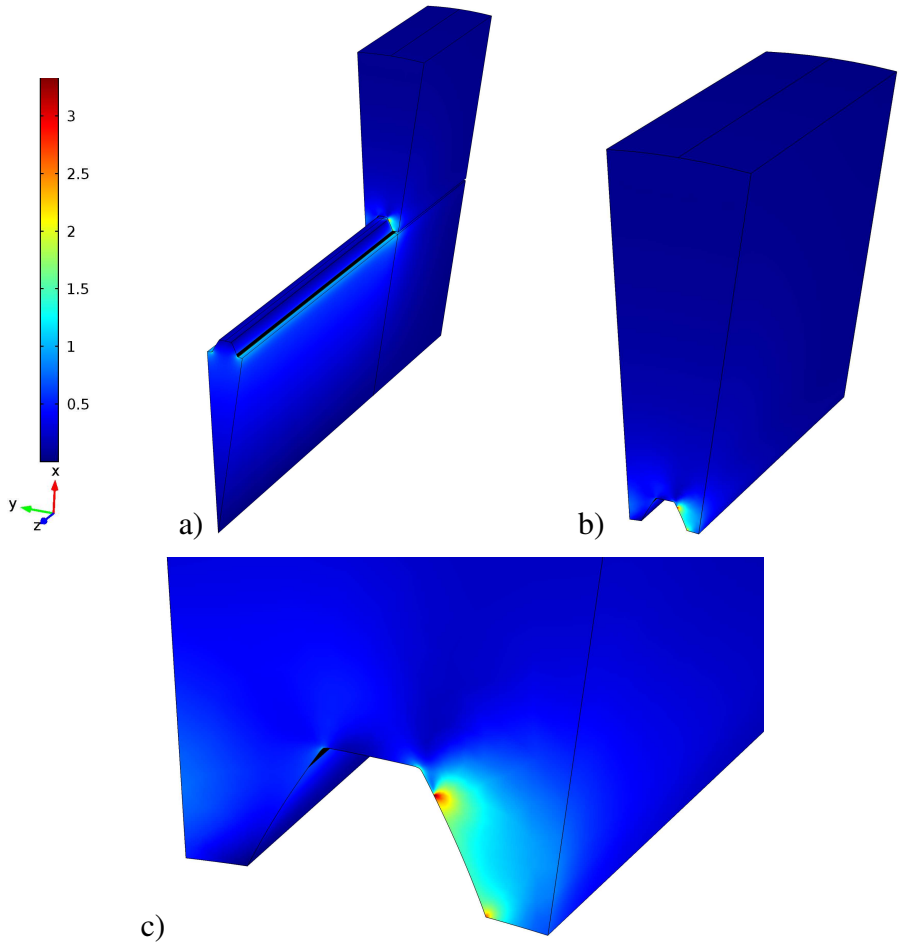

Figure 7: Illustration of variation in von Mises stress, the stress is scaled by the nominal von Mises stress. a) Full finite element model with one teeth b) Zoom of part of hub included in the modelling c) Zoom of the point with high stress.

To model the stress arising from the torque transfer between shaft and hub a number of points are important and needs to be taken into account for the numerical modelling. Especially also in relation to a subsequent optimization procedure.

Important points in modelling torsion are:

- Friction
- Load and boundary conditions
- Thickness and diameter of hub
- Tolerances
- Place to evaluate stress for optimization

In the points highlighted nothing is mentioned in relation to the FE modelling, which however also is highly important and stress convergence check is necessary. The five bullet point are discussed in (Pedersen 2021) so only a short discussion is given in the present paper.

The friction does have an influence on the result so this needs to be included in the modelling, the friction is here modelled using Coulomb friction and the friction coefficient is throughout the paper selected to be $\mu = 0.1$.

The connection loading is assumed to be purely torsional. In Figure 7 the torque is applied to the shaft and the hub is fixed, alternatively the torque could be applied to the hub and the shaft could be fixed. Depending on the distance to the contact from the application points, i.e. the shaft length relative to the hub thickness and the hub outer diameter relative for the reference diameter the result will not be identical. If the shaft length and the hub outer diameter are selected sufficiently large the influence from switching the load and boundary condition is neglectable. So bullet point 2 and 3 are to some extend related.

The tolerances was in (Pedersen 2021) shown to have a significant influence on the stress concentration size, some similarities in the stress distribution for limited tolerances where found. The production precision of involute splines are comparable to that of gears and it can therefore be argued that we can neglect the influence from tolerances in the modelling. We therefore assume a perfect fit.

In order to reduce the number of elements in the FE model for optimization iteration purposes, the hub thickness is reduced to $0.1d_B$. By doing this the maximum stress is increased but the stress distribution is primarily scaled. The optimization can then be performed with the reduced hub thickness and the resulting optimized design can then be verified for a thicker hub if needed. The stress evaluation used for the optimization is still important. In Figure 8 the stress in the hub is shown for the side and the centre.

In Figure 8 we clearly see that there is a large difference in the stress. This can also be seen in Figure 9 which shows the stress along the two lower boundaries in Figure 8. In Figure 9 the stress is shown as a function of the arc length, s. For the outer rim (bottom boundary of Figure 8a) the stress is shown from right to left, and for the centre rim (bottom boundary of Figure 8b) the stress is shown from left to right, as indicated on Figure 8. Relative to Figure 8 the mesh is refined. That the mesh is refine result in an maximum stress increase.

For both curves we see two singularity points, with mesh refinements the stress value at these points will not converge. For the non-contacting part we see that the stress level is similar for both the outer rim and the centre rim. For the outer rim we further have that the maximum stress is more sensitive to mesh refinements. Due to the similarity of the two curves it is therefore selected to use the stress along the centre rim in the optimization, i.e. minimizing the maximum stress on the centre rim. The mesh used for the results in Figure 9 is shown in Figure 10.

In the next section optimization of the connection is performed. Because the stress cannot be converged at the singularity points it is important that doing the optimization procedure the

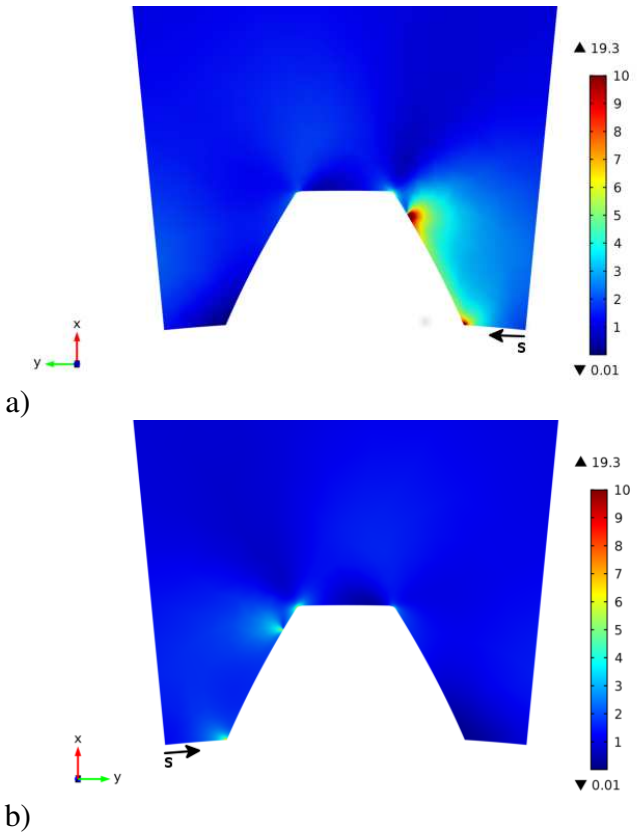

Figure 8: Stress in hub, the stress is scaled by the nominal von Mises stress and for illustration purpose the colour scale stops at 10 although the maximum value in 19.3. a) Side of hub (axial end surface). b) Centre of hub (halfway through the axial length).

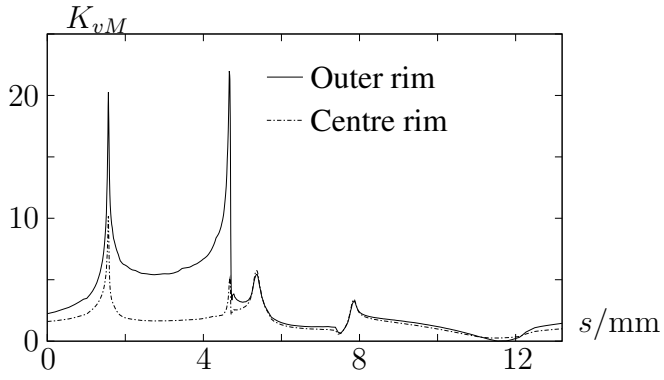

Figure 9: Stress in bottom rim of hub, the stress is scaled by the nominal von Mises stress. a) Outer side of hub. b) Centre of hub.

mesh size is kept fixed. By doing this we can see the relative improvement in the stress level. For this reason the optimization can be performed with a more coarse mesh than the one in Figure 10, because we can verify the stress level for the resulting design by a final mesh refinement.

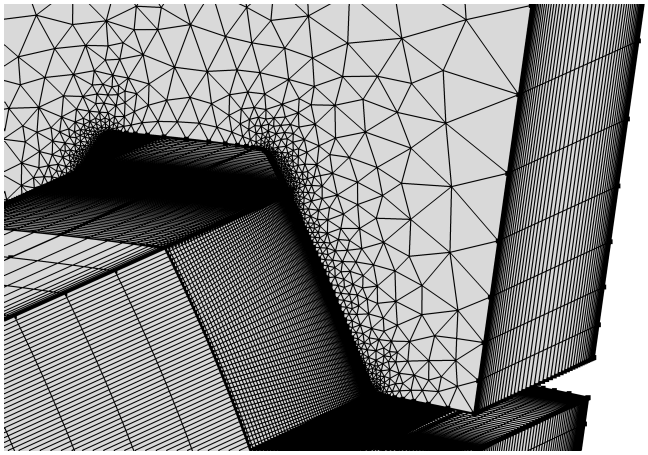

Figure 10: Zoom of FE mesh used.

5 Optimized design

In the existing involute spline design the primary reason for the highest stresses is the singularity points where there is a contact run-out. This run-out happens at the teeth tip for both the hub and shaft. In the axial direction we also have a run-out along the full involute part, this is seen by the elevated stress level in Figure 9 for the outer rim. One way to reduce this effect is to reduce the stiffness as done in e.g. (Pedersen 2016).

5.1 Improving existing involute spline design

The idea is to change the design only where we have no contact, in this way the modified design can function with the existing standard design. The object is to reduce the stiffness at the run-out without causing a new stress concentration. This modification can be realized in many ways. Here a relatively simple approach with 4 design parameters is used as shown in Figure 11. The stiffness reduction is primarily controlled by the value of r_i and r_o (see Figure 11). The fillet radius values r_{fi} and r_{fo} are added to avoid the stress concentration at the internal corners. These design modifications can be achieved without interfering with the fine tolerances in the involute design production.

Due to the small number of design parameters a parameter study can be made for reducing/optimizing the stress level, i.e. no design sensitivities are applied. In Figure 12 the stress of the optimized design is shown and in Figures 13 and 14 the stress along the outer and the centre rim is shown for the optimized design and the initial design, respectively. The mesh refinement for both cases is identical. The optimization focus is here to reduce the high stress level on the outer rim. From structural optimization it is known that if the stress is constant along major parts of the design domain then this indicates that the design is optimal. In Figure 12 we note that the stress is to some extent constant over the contact indicating that the design is optimized and with a maximum scaled stress of 8.5.

Compared to Figure 9 we in Figures 13 and 14, only show the stress along half the rim where we have the highest stress and the contact. The mesh used for the optimization is more coarse than the one shown in Figure 10 leading to that the stress at the singularity points are evaluated to be slightly lower for the initial design. The relative improvement between initial design and optimized design is seen in the figures due to that the same mesh refinement is used for the both initial and optimized design. The optimized design parameter values are

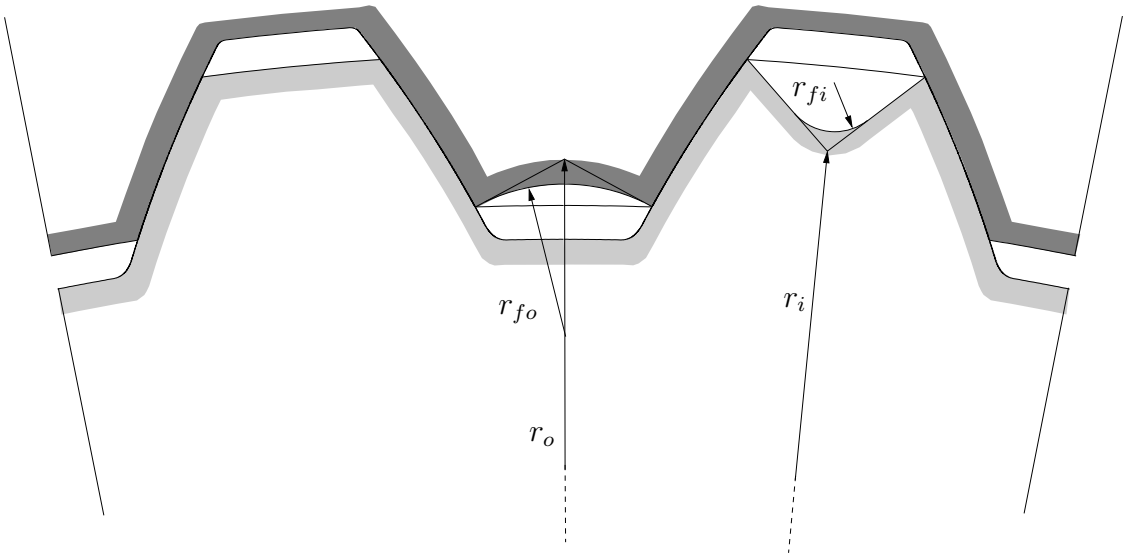

Figure 11: Part of spline connection, $z = 32$, $M = 3\text{mm}$, from (DIN 5480-16 2006). The design modification are shown on one teeth on shaft and one teeth on hub.

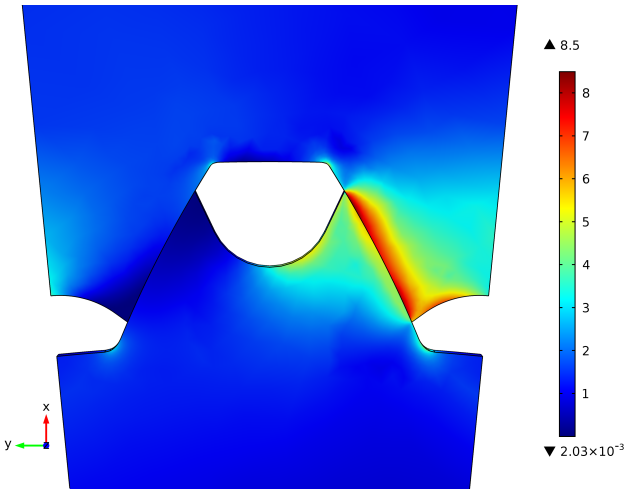

Figure 12: Stress in hub and shaft, the stress is scaled by the nominal von Mises stress. In the view the side of hub is shown.

$$r_i = 46\text{mm}, \qquad r_{fi} = 1.3\text{mm}, \qquad r_o = 48\text{mm}, \qquad r_{fo} = 2.0\text{mm}$$

In Figure 14 we see that for the centre rim the maximum stress is no longer found in the contact but in the corner corresponding to point a in Figure 5, we also have that the stress is higher in the fillet (with radius r_{fo}) than in the contact. For the outer rim we, as seen in Figure 13, have the highest stress in the contact and the stress is relatively constant. For the optimized design we have a significant reduction in the maximum stress on the outer rim by 45%.

For the centre rim the stress reduction is 24%. If further stress reductions should be made to the stress at the centre rim we need also to look at the corner (point a in Figure 5), this will not be attempted here instead we present a new design.

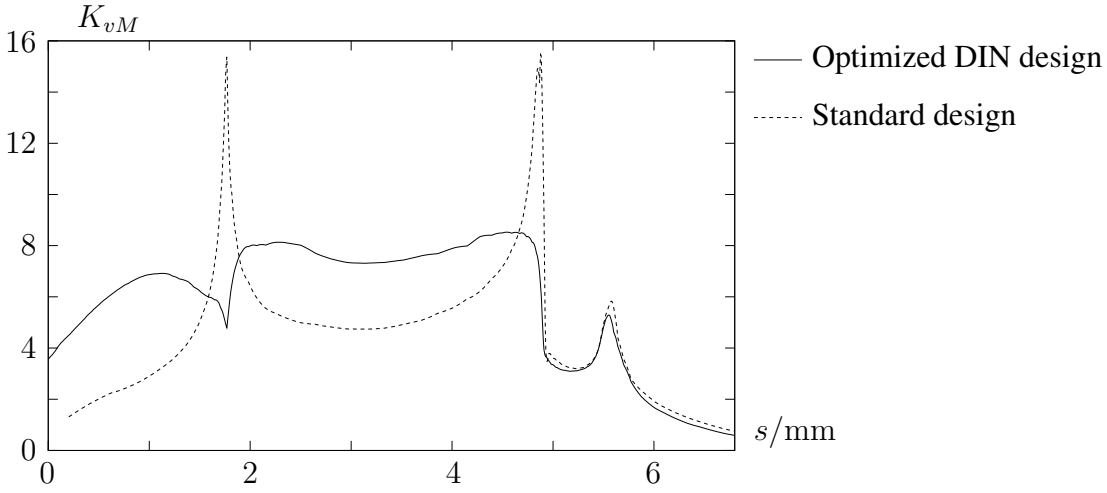

Figure 13: Stress in half bottom rim of hub outer side, the stress is scaled by the nominal von Mises stress.

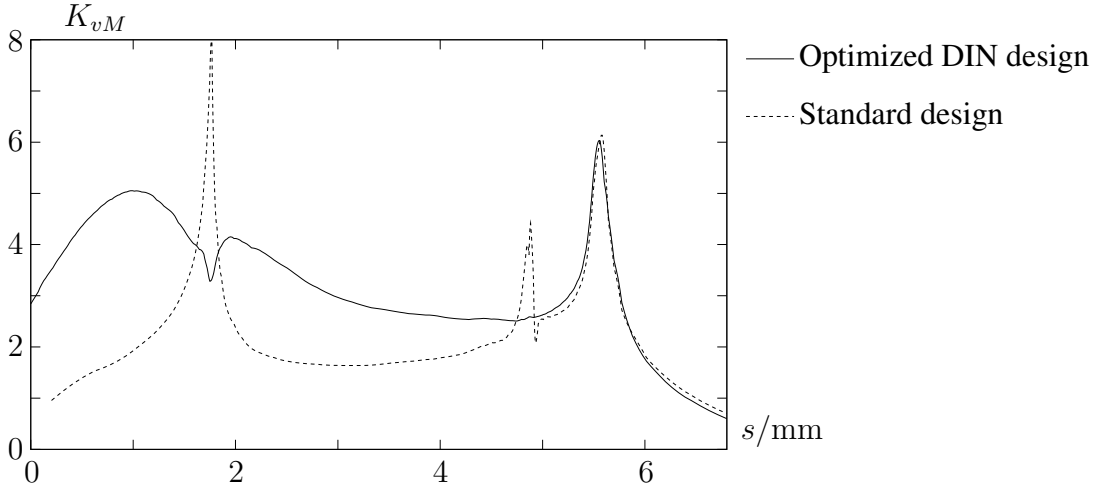

Figure 14: Stress in half bottom rim of hub centre, the stress is scaled by the nominal von Mises stress.

5.2 New spline design

The possibilities for a new design are large. It is clear that with total design freedom we can reduce the stress further compared to the modified original design. Using e.g. higher teeth leads to a significant reduction of the maximum stress. In order to make a comparison with the DIN design the following constrains to the design are used

- Contact takes place for radius values between $r_{ci} = (z/2 - 0.45)M = 46.65\mathrm{mm}$ and $r_{co} = (z/2 + 0.65)M = 49.95\mathrm{mm}$)
- Design domain for hub is within radius values r_{ci} and r_{co}
- Design domain for shaft is within radius values $r_r = (z/2 - 0.65)M = 46.05\mathrm{mm}$ and r_{co}

An initial idea could be to use an angle of $\pi/2$ between load and position vector (similar to straight sided splines) in the contact and reduce tooth tip stiffness as done in the previous design modification, this could lead to a design as indicated in Figure 15

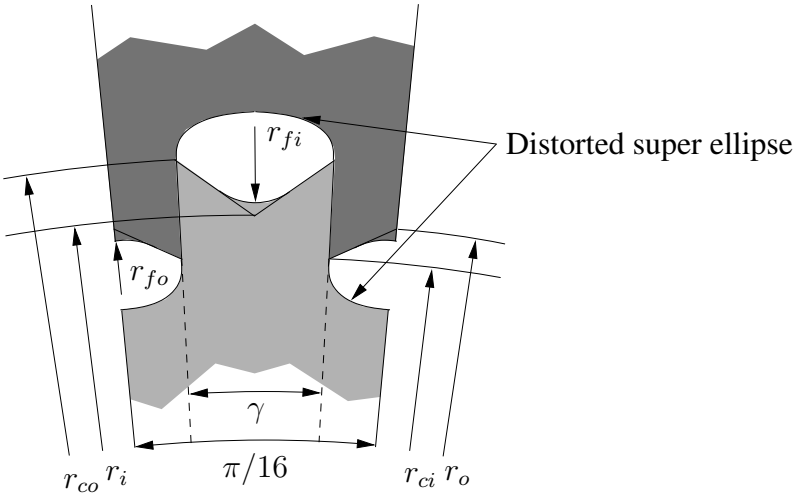

Figure 15: Suggested design with an angle of $\pi/2$ between load and position vector.

However numerical experiments with this design has shown that the stress level is higher than the initial DIN design.

Instead a design based on the super ellipse is proposed. The new design is illustrated in Figure 16.

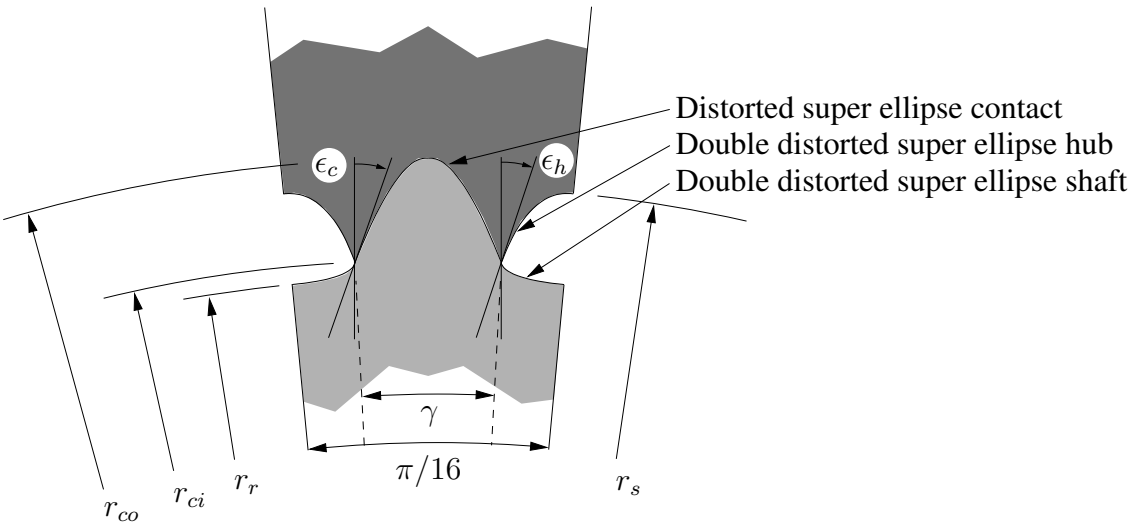

Figure 16: Suggested design with super ellipse.

In the design a distorted super ellipse is used for the contact geometry, and a double distorted super ellipse is used for the tooth root in the shaft and for the stiffness reduction of the teeth on the hub.

The design variables are γ, ϵ_c, ϵ_h, r_s and the super elliptic power η_c for the super ellipse for the contact and the super ellipse for the root, and finally we have the super elliptic power η_h for the hub. In total the number of design variables is 6. The results are relatively insensitive to the super elliptic power of the root shape in the hub and therefore here we assume it identical to the power in the contact geometry.

For the root (in the hub) to the left in Figure 16 the super ellipse is in parametric form given as

$$X = a\cos(t)^{(2/\eta_s)}, \qquad t \in [0 : \frac{\pi}{2}] \tag{10}$$

$$Y = -b\sin(t)^{(2/\eta_s)}, \qquad t \in [0 : \frac{\pi}{2}] \tag{11}$$

η_s is the super elliptic power and a and b are the principal half axes, which are fixed by the design constraints. The super ellipse shape is double distorted, to fit the left boundary and by the design variable ϵ_c. The super ellipse distorted only by the angle ϵ_c is in parametric form given as

$$X_d = (a - b\sin(t)^{(2/\eta_s)}\tan(\epsilon_c))\cos(t)^{(2/\eta_s)}, \qquad t \in [0 : \frac{\pi}{2}] \tag{12}$$

$$Y_d = -b\sin(t)^{(2/\eta_s)}, \qquad t \in [0 : \frac{\pi}{2}] \tag{13}$$

The super ellipse and the distorted super ellipse are illustrated in Figure 17, where also the angle ϵ_c is defined.

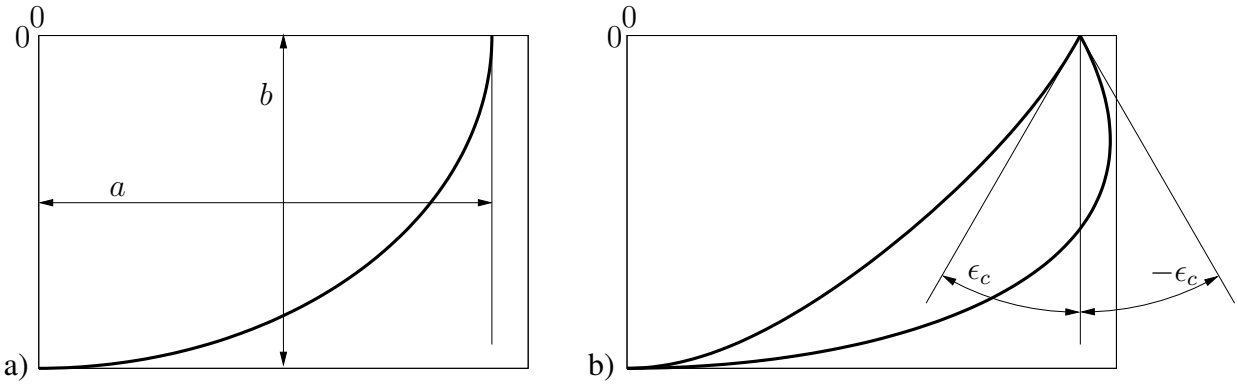

Figure 17: a) Super ellipse. b) Distorted super ellipse.

Applying the distortion angle $\epsilon_t = \pi/32$ at the other end of the ellipse (at point $(0. - b)$) we finally have the double distorted super ellipse in parametric form.

$$X_{dd} = (a - b\sin(t)^{(2/\eta_s)}\tan(\epsilon_c))\cos(t)^{(2/\eta_s)}, \qquad t \in [0 : \frac{\pi}{2}] \tag{14}$$

$$Y_{dd} = -(b - (a - b\sin(t)^{(2/\eta_s)}\tan(\epsilon_c))\cdot \cos(t)^{(2/\eta_s)})\tan(\epsilon_t))\sin(t)^{(2/\eta_s)}, \qquad t \in [0 : \frac{\pi}{2}] \tag{15}$$

By simple transformations the analytical shape for the distorted and double distorted super ellipses is used for the shape of the proposed design.

Also here due to the small number of design parameters a parameter study is made for reducing/optimizing the stress level. In Figure 18 the stress of the optimized design is shown and in Figures 19 and 20 the stress along the outer and the centre rim is shown for the optimized design and the initial DIN design, respectively. The mesh refinement for both cases is identical. In Figure 18 we note that the design has a maximum scaled stress of 7.07, corresponding to a 54% reduction in the maximum stress. For the centre rim the stress reduction is 53%, i.e. comparable to the reduction on the outer rim. The values of the design variable for this design are

$$\gamma = 0.041\pi, \qquad \eta_c = 2.29, \qquad \epsilon_c = 0.49$$
$$r_s = 49\text{mm}, \qquad \eta_h = 1.90, \qquad \epsilon_h = 0.16$$

This improvement should be compared to the result for the improved existing design where the improvements were 45% on the outer rim and 24% on the centre rim. All improvements are given relative to the standard design.

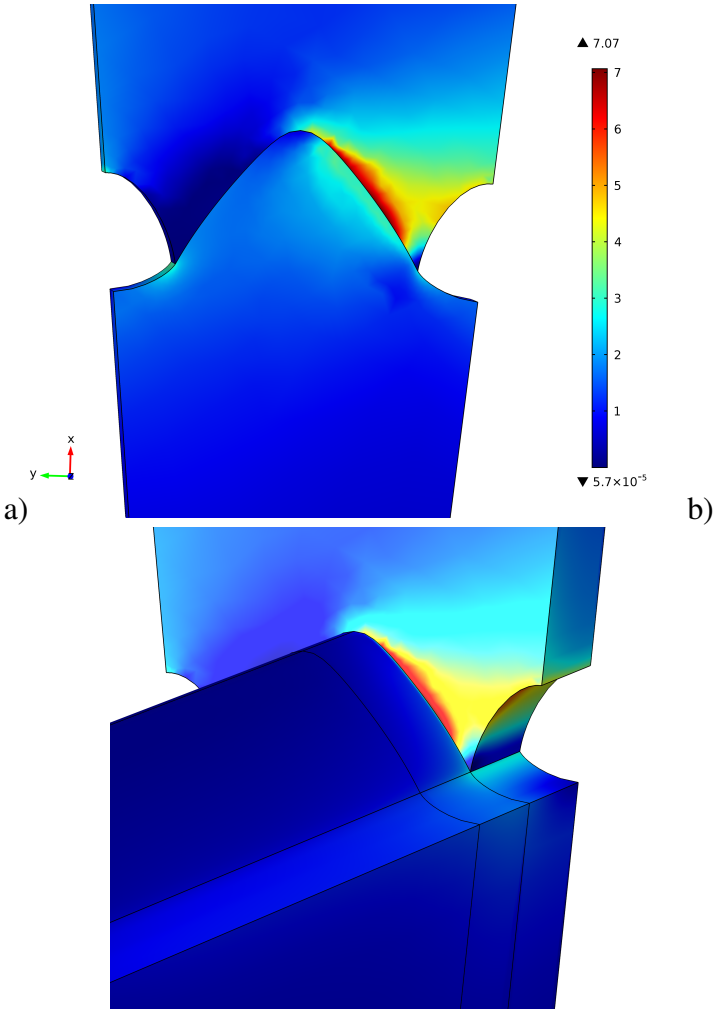

Figure 18: Stress in hub and shaft, the stress is scaled by the nominal von Mises stress. a) End surface of the hub. b) 3D view.

The presented optimized design is based on the selected parameterization with 6 design variables. With a parameterization with more design variables it is probably possible to reduce the stress level even further. However with the simple analytical shape presented here the found stress reduction is significant. If the stress level is compared to the optimized trilobe design presented in (Pedersen 2021) we find a significantly lower stress for the design presented in the present paper.

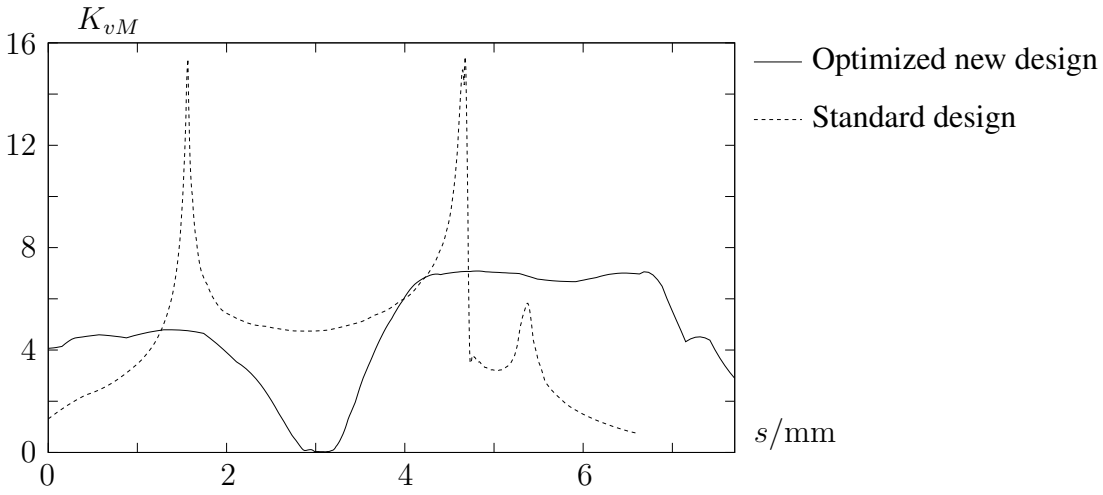

Figure 19: Stress in half bottom rim of hub outer side, the stress is scaled by the nominal von Mises stress.

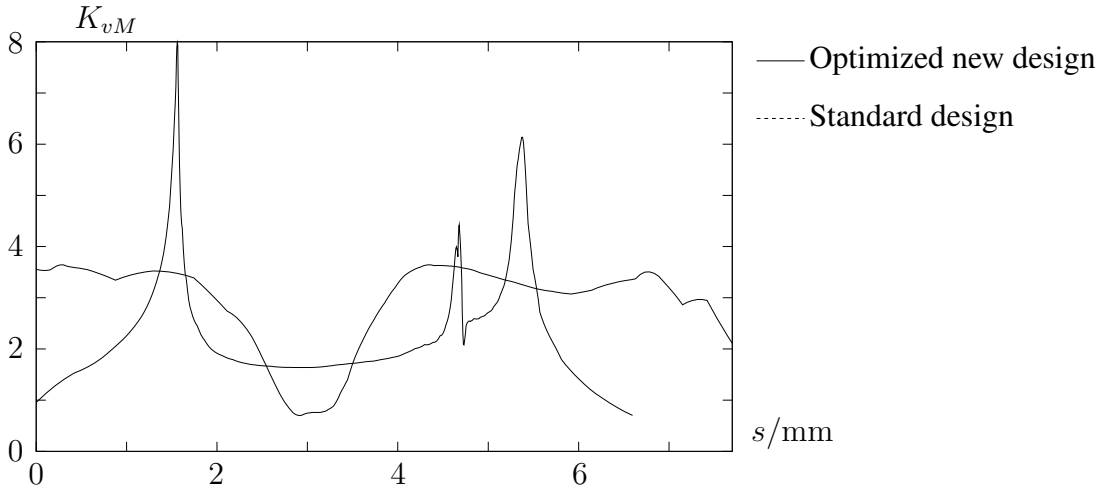

Figure 20: Stress in half bottom rim of hub centre, the stress is scaled by the nominal von Mises stress.

6 Conclusion

In the present paper it is shown how the strength of a shaft hub connections can be improved significantly relative to the standard involute spline.

Two designs are proposed. The first design is a modification to the original standard involute spline connection. The contact geometry is not changed so the revised design can work with the original design. The numerical results for a shaft diameter of $100\mathrm{mm}$ show that the maximum stress on the rim of the hub can be reduced by 45% while the reduction at the centre is 24% .

The second design proposal is an alternative to the involute spline. The design is based on the super ellipse. The shape it therefore described by a simple analytical expression. For the new design a stress reduction of 54% is found on the rim of the hub while the reduction at the centre is 53%. The second design show and overall significant stress reduction relative to standard design and the shape is given by a simple super elliptic parameterization.

Acknowledgement
For discussions and suggestions I wish to thank Prof. Peder Klit.

References

Barrot, A., Paredes, M. & Sartor, M. (2009), 'Extended equations of load distribution in the axial direction in a spline coupling', *Engineering Failure Analysis* **16**(1), 200–211.

Barsoum, I., Khan, F. & Barsoum, Z. (2014), 'Analysis of the torsional strength of hardened splined shafts', *Materials and Design* **54**, 130–136.

Benatar, M., Talbot, D. & Kahraman, A. (2017), 'An experimental investigation of the load distribution of splined joints under gear loading conditions', *Journal of Advanced Mechanical Design, Systems and Manufacturing*.

Chase, K. W., Sorensen, C. D. & Decaires, B. J. (2010), 'Variation analysis of tooth engagement and loads in involute splines', *Ieee Transactions on Automation Science and Engineering* **7**(4), 5332271, 746–754.

COMSOL AB (1986 -), Stockholm, Sweden, www.comsol.com.

Czyzewski, T. & Odman, M. T. (1988), 'Analysis of contact stress and deformation in a trilobe polygonal connection', *Journal of Engineering for Industry* **110**(3), 212.

DIN 32711 (1979), 'Polygonprofile P3G; antriebselemente (in German)'.

DIN 32712 (1979), 'Polygonprofile P4C; antriebselemente (in German)'.

DIN 5480-1 (2006), 'Splined connections with involute splines based on reference diameters - part 1: Principles (German standard)'.

DIN 5480-16 (2006), 'Splined connections with involute splines based on reference diameters - part 16: Tools (German standard)'.

DIN 6885-1 (1968), 'Paßfedern nuten (in German)'.

DIN ISO 14 (1986), 'Keilwellen-verbindungen mit geraden flanken und innenzentrierung'.

Hong, J., Talbot, D. & Kahraman, A. (2015), 'Effects of tooth indexing errors on load distribution and tooth load sharing of splines under combined loading conditions', *Journal of Mechanical Design, Transactions of the Asme* **137**(3), 032601.

Kahn-Jetter, Z. L. & Wright, S. (2000), 'Finite element analysis of an involute spline', *Journal of Mechanical Design, Transactions of the Asme* **122**(2), 239–244.

Kahn-Jetter, Z. L., Hundertmark, E. & Wright, S. (2000), 'Comparison of torque transmitting shaft connectivity using a trilobe polygon connection and an involute spline', *Journal of Mechanical Design, Transactions of the Asme* **122**(1), 130–135.

Leykin, A. S. & Starichneva, A. F. (1975), 'Stress-concentration and distribution during torsion of splined shafts with involute tooth profile', *Russian Engineering Journal* **55**(11), 19–23.

Pedersen, N. L. (2010), 'Stress concentrations in keyways and optimization of keyway design', *Journal of Strain Analysis for Engineering Design* **45**(8), 593–604.

Pedersen, N. L. (2011), 'Optimization of straight-sided spline design', *Archive of Applied Mechanics* **81**(10), 1393–1407.

Pedersen, N. L. (2015), 'Minimizing tooth bending stress in spur gears with simplified shapes of fillet and tool shape determination', *Engineering optimization* **47**(6), 805–824.

Pedersen, N. L. (2016), 'On optimization of interference fit assembly', *Structural and Multidisciplinary Optimization* **54**(2), 349–359.

Pedersen, N. L. (2019), 'Stress concentration and optimal design of pinned connections', *Journal of Strain Analysis for Engineering Design* **54**(2), 95–104.

Pedersen, N. L. (2021), 'On optimal stress for shaft-hub connections (polygon connections)', *Journal of Strain Analysis for Engineering Design* **56**(4), 195–205.

Tjernberg, A. (2001), 'Load distribution in the axial direction in a spline coupling', *Engineering Failure Analysis* **8**(6), 557–570.

Volfson, B. P. (1982), 'Stress sources and critical stress combinations for splined shaft', *Journal of Mechanical Design-transactions of the Asme* **104**(3), 551–556.

Wendler, J. & Schlecht, B. (2016), 'Stress concentration and fatigue strength of involute spline shafts and couplings', *Power Transmissions - Proceedings of the International Conference on Power Transmissions, Icpt 2016* **0**(191039), 311–318.

Wink, C. H. & Nakandakari, M. (2013), 'Influence of gear loads on spline couplings', *American Gear Manufacturers Association Fall Technical Meeting 2013* pp. 287–300.

Yoshitake, H. (1962), 'Photoelastic stress analysis of the spline shaft', *Bulletin of Jsme* **5**(17), 195–201.